




Lagrangian descriptors for the Bunimovich stadium billiard

Gabriel G. Carlo ^{1,*}, J. Montes ^{2,3,†} and F. Borondo ^{2,3,‡}

¹*Comisión Nacional de Energía Atómica, CONICET, Departamento de Física, Av. del Libertador 8250, 1429 Buenos Aires, Argentina*

²*Departamento de Química, Universidad Autónoma de Madrid, Cantoblanco, 28049 Madrid, Spain*

³*Instituto de Ciencias Matemáticas (ICMAT), Cantoblanco, 28049 Madrid, Spain*



(Received 7 October 2021; accepted 24 December 2021; published 12 January 2022)

We apply the concept of Lagrangian descriptors to the dynamics on the Bunimovich stadium billiard, a two-dimensional ergodic system with singular families of trajectories, namely, the bouncing ball and the whispering gallery orbits. They play a central role in structuring the phase space, which is unveiled here by means of the Lagrangian descriptors applied to the associated map on the boundary. More interestingly, we also consider the open stadium, which in the optical case (Fresnel's laws) can be directly related to recent microlaser experiments. We find that the structure of the emission profile of these systems can be easily described thanks to the open version of the Lagrangian descriptors.

DOI: [10.1103/PhysRevE.105.014208](https://doi.org/10.1103/PhysRevE.105.014208)

I. INTRODUCTION

The precise characterization of the structure of the phase space of chaotic systems is of importance in many areas, and at the same time a nontrivial task. In particular, the description of the stable and unstable manifolds associated to unstable periodic orbits (POs) has recently benefited from the introduction of a classical measure, the Lagrangian descriptors (LDs) [1]. They can be easily evaluated [2–4] in comparison with other methods like obtaining a Poincaré surface of section. Their applications range from chemical dynamics [5–9] to abstract mathematical objects like area preserving maps, dynamical systems for which discrete LDs have been devised and applied to prototypical cases, like that of the Arnold's cat [10]. In this context, chaotic saddles associated to open [11] or scattering [12] systems have been studied by a redefinition of the LDs for open maps in [13]. In fact, eliminating the trajectories going through an “opening” in phase space (a given finite area region [14]) leaves just a repeller, which is a fractal invariant set. The redefined measure adapts the LD tool in order to reveal the structure embedded in these repellers while keeping its simplicity. As a result, the homoclinic tangles associated to POs belonging to the repeller can be very efficiently identified. This is a difficult task in general, but we have shown how it can be easily done in the case of the open tribaker map [13], where the obtained results can be contrasted with those of the associated simple symbolic dynamics. This allowed one to demonstrate once more the usefulness of LDs.

It is of great interest for both theoretical and experimental reasons to extend these concepts to realistic situations. This can be achieved, for example, by considering billiard systems

that are used as excellent models for resonator cavities in many devices. Moreover, it is also important to implement more general ways to make them open, going beyond the just purely projective (complete) openings or abstract partially open regions (see, for example, Ref. [13]). A very relevant example is the escape of trajectories or rays following Fresnel's laws [15], which leads to many interesting mathematical properties and is directly applicable to optical microdisk cavities with deformed boundaries [16].

In this paper, we apply LDs to a two-dimensional ergodic billiard [the paradigmatic Bunimovich stadium (BS)]; more specifically, to the corresponding map on the boundary using Birkhoff coordinates, which captures all the essential features of the dynamics. We find that two families of singular orbits, namely, bouncing ball orbits (BBOs) and whispering gallery orbits (WGOs), provide the foundations of the chaotic structure associated to the closed system phase space. Moreover, we open the system by letting some trajectories escape according to both a completely projective and also an optical mechanism. The latter corresponds to one of the cavities used in very recent microlaser experiments [17]. The enhanced vision of POs and their associated homoclinic tangles provided by LDs for open maps allowed us to identify which of the shortest ones are responsible for the main properties of the emission in experimental situations. This throws new light on the future design of these devices, as well as to all kinds of resonator cavities (like microwave, for example). Also, it reveals which kind of orbits outside of the purely projective repeller could be relevant in the semiclassical theory of short POs for partially open systems [18,19].

We have organized this paper in the following way: In Sec. II we define the LDs used, we describe the main properties of the BS, and also those of the corresponding map on the boundary written in Birkhoff coordinates. In Sec. III we apply this definition to unveil the underlying structure of the main manifolds that characterize the BS phase space in the closed case and more importantly, to explain the properties of

*carlo@andar.cnea.gov.ar

†jmontes.3@alumni.unav.es

‡f.borondo@uam.es

the emission in the optically open scenario. Our conclusions are finally presented in Sec. IV.

II. LAGRANGIAN DESCRIPTORS AND THE BUNIMOVICH STADIUM BILLIARD

Since chaotic maps are prototypical models that capture all the essential features of chaotic dynamics, we restrict ourselves to them in this work. Open maps are obtained by considering a region of escape; in our case a two-dimensional “hole” in our phase space expressed in terms of canonical variables (q and p) by the function $F(q, p)$, which will be defined at the end of this section. This gives rise to an invariant set, the fractal dimensional repeller, given by the intersection of the forward and backward trapped sets. These sets are built by computing the trajectories that never escape either in the past or in the future, respectively. In order to obtain a representation of the repeller we discretize the phase space into an arbitrary finite number of smaller areas called X_i . Then, the invariant set can be expressed in terms of a measure $\mu(X_i)$, which varies in these X_i regions. To compute $\mu(X_i)$ we evaluate the average intensity $\langle I_{t,i} \rangle$ for every X_i , in the limit $t \rightarrow \infty$. This average $\langle \cdot \rangle = \sum_{(q_i, p_i) \in X_i}^N / N$ is performed over a large number N of random initial conditions inside a given X_i . In fact, for any pair of initial conditions $(q_i, p_i) \in X_i$ we assign an initial intensity $I_{0,i}^{(q,p)} = 1$. This intensity, which is a kind of weight for each trajectory, evolves according to $I_{t+1,i}^{(q,p)} = F(q, p) I_{t,i}^{(q,p)}$ being updated at every hit on the boundary. We emphasize that the function $F(q, p)$ here is arbitrary and fully characterizes the properties of the phase-space opening. A finite time approximation to this measure (and the repeller) can be obtained as $\mu_{t,i}^b \cap \mu_{t,i}^f$, where $\mu_{t,i}^{b,f} = \langle I_{t,i} \rangle / \sum_i \langle I_{t,i} \rangle$ are the finite time backward and forward trapped sets.

To understand the structure of the repeller, we use in this work the definition of LDs for open maps of [13], adding the contribution of N trajectories $\{q_t, p_t\}_{t=-t_f}^{t=t_f}$ at each X_i , where $t \in \mathbb{N}$, as

$$\begin{aligned} \text{LD} &= \text{LD}^- \times \text{LD}^+ \\ &= \sum_{t=-t_f}^{t=1} (|q_{t+1} - q_t|^a + |p_{t+1} - p_t|^a) I_t \\ &\quad \times \sum_{t=0}^{t=t_f-1} (|q_{t+1} - q_t|^a + |p_{t+1} - p_t|^a) I_t, \end{aligned} \quad (1)$$

and normalizing the LD to 1. We use this definition of discrete LDs for open maps, even for the area-preserving case, since the structure of the manifolds is also better identified in this way. We take a $2^8 \times 2^8$ square grid on the torus, $N = 10^3$ trajectories at each region X_i defined by this grid, and $t_f = 30$ (unless otherwise specified).

A word regarding the significance of LDs is in order here. This tool is ideal to reveal the phase-space structures that are embedded in different regions, being them regular or chaotic. In particular, they are able to identify in a clear-cut way the structure of homoclinic tangles associated to POs in chaotic domains. This is difficult to achieve by using Poincaré maps. They are also suitable to see chains of regular islands in the

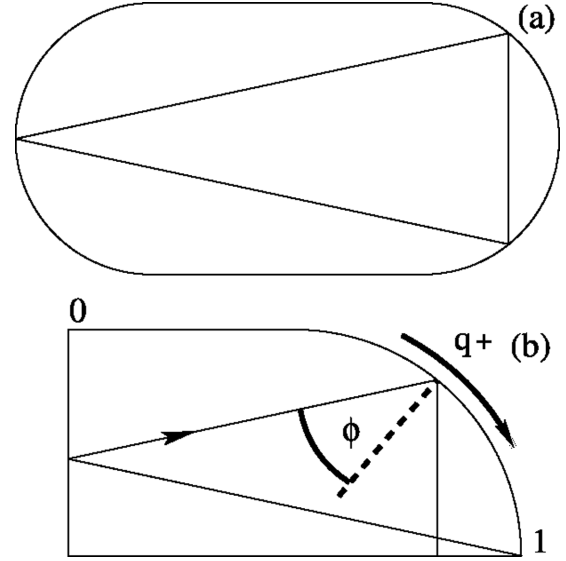


FIG. 1. (a) Bunimovich stadium billiard with one of the shortest POs as an example. (b) Quarter (desymmetrized) billiard with the corresponding version of the PO shown in (a). Notice the positive direction of the q coordinate indicated by the curved arrow, and the tangential momentum $p = \sin \phi$ also positive in this case.

mixed part of phase space and also very elusive structures such as cantori. Moreover, they are very easy to calculate compared to other representations since they rely essentially on trajectories’ arc lengths. It is also important to clarify the role of parameter a appearing in Eq. (1). This corresponds to taking the a norm, which for $a = 1$ is the so-called taxicab or Manhattan norm, i.e., the distance corresponding to moving in a rectangular grid to the final point. For different values it works as a sensitivity parameter that sometimes allows one to single out different underlying phase-space structures.

The map to which we apply this measure is the surface of section corresponding to the phase space of the BS, shown in Fig. 1(a). Notice that any differentiable curve equipped with a coordinate q and another p orthogonal to it can be used for our purposes. When considering billiards that are bounded by rigid walls, one usually takes the boundary to construct the surface of section in Birkhoff coordinates, i.e., the boundary arc length q and the tangential momentum p at the bounces. In this case the discrete times t of the map correspond to the instants at which the trajectories hit the walls. In fact, we consider just the boundary of the quarter (desymmetrized) billiard measured from the upper-left corner and up to the right one (corresponding to $q = 0$ and $q = 1$, respectively), and the tangential momentum $p = \sin \phi$, where ϕ is the incident angle with respect to the normal, as indicated in Fig. 1(b). This reduction to the fundamental domain captures all the dynamical properties of the full BS, making at the same time a much more efficient use of the computational resources by eliminating redundant calculations.

Finally, we define the opening function to obtain the open map on the boundary as the composition of the corresponding closed one with the function. In this work, we consider two different functions in phase space. First (for illustrative purposes) $F_R(q, p)$, with R being a reflectivity parameter that

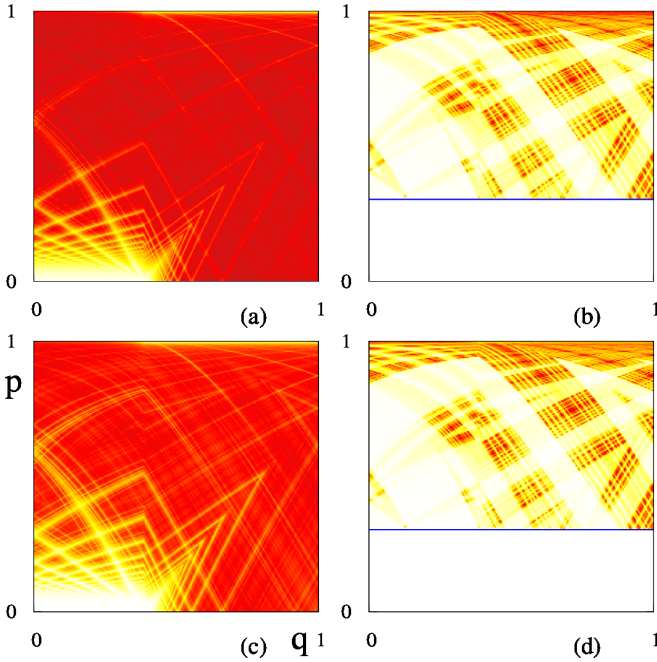


FIG. 2. LD for the Bunimovich stadium map on the boundary. The left panels correspond to the closed Bunimovich stadium, and the right ones show the results for the completely open case with $n = 3.3$. The upper panels [(a) and (b)] correspond to $a = 0.3$ while the lower ones [(c) and (d)] are for $a = 0.9$. In the right panels the value of p_{tr} is indicated by means of blue (black) horizontal lines. The color code used here and in the following similar figures goes from light to dark orange signaling lower to higher values of LD.

goes from complete escape for $R = 0$ to the closed map when $R = 1$ [19]. The opening region, in this case, is the domain given by the angle of total internal reflection which translates into the corresponding $p_{tr} = 1/n$ value by using Snell's law, where n is the refraction index of the material from which the BS cavity is fabricated. As such, this region is delimited by $-p_{tr} \leq p \leq p_{tr}$ for all q . More precisely, we take a constant function given by the value of R in the opening and 1 elsewhere. In this case, we select a complete opening, i.e., $R = 0$ (some amount of the incoming trajectories is reflected for other values). The second reflection mechanism is given by a Fresnel-type reflectivity function [15] that involves a partial escape at a dielectric interface. For transverse magnetic polarization it is given by

$$F_n(q, p) = \left[\frac{\sqrt{1 - (np)^2} - n\sqrt{1 - p^2}}{\sqrt{1 - (np)^2} + n\sqrt{1 - p^2}} \right]^2, \quad (2)$$

the opening region being the same as in the previous case. The function $F_n(q, p)$ of Eq. (2) corresponds exactly to the situation arising in experimental setups, in particular for the case of microlasers. In fact, this is a widely used expression to obtain correct predictions that solve differences with measured data arising when just considering the complete opening of the first case. These differences are critical for quantum calculations where the usual Weyl law needs to be carefully considered.

III. RESULTS

We first apply LDs to study the closed BS. The results are presented in Figs. 2(a) and 2(c) for two different values of the parameter in Eq. (1): $a = 0.3$ and 0.9 , respectively. We have evaluated the behavior of LD varying the a norm in order to check if there is any important dependence on it, when identifying the structures in the phase space. Our results show that aside from an enhancement of some structures and a blurring of others, no qualitatively different features can be found due to the variation of the used norm. Moreover, it is clear that the structure of the chaotic phase space is mainly dominated by the manifolds emanating from the BBOs family. This is a family of singular, i.e., marginally stable trajectories, that constitute a continuous set along the lower values of the boundary coordinate (corresponding to the straight segment of the wall), impacting at an angle $\phi = 0$. Also, the WGOs that develop mainly along the boundary with very large values of ϕ , play an important part in the phase-space structure. Indeed, they give rise to the next relevant sets of manifolds emanating from them, which are essentially located in a very narrow region corresponding to the circular part of the boundary near $p = 1$. Next, in Figs. 2(b) and 2(d) we present the effect on this set of manifolds considering a complete opening in the BS for $n = 3.3$. As can be seen, the BBOs are completely wiped out along with their manifolds, while the WGOs survive in the repeller. Actually, the latter are the dominating POs (with their manifolds) for this case, completely ruling the structure of the phase space.

We now further analyze the partially (Fresnel) open BS in order to characterize the structure of the repeller beyond the clear dominance of the WGOs. The top and bottom panels of Fig. 3 show the results for two extreme cases, corresponding to low and high values of n , respectively. In Fig. 3(a) we show the case $n = 1.5$ ($a = 0.3$) where the p_{tr} value is high. There is a big opening through which most of the trajectories escape and the only relevant surviving ones are the WGOs with a few more orbits contributing to the structure of the repeller. To find out which are the most significant, we take $a = -0.3$ and eliminate the WGOs [see the results in Fig. 3(b)]. This leaves just one relevant small area that is far from the p_{tr} line. On the other hand, at the other extreme, i.e., $n = 5.0$, we see that although WGOs are again the main component of the repeller [see Fig. 3(c) where we used $a = 0.3$], there are many more POs and associated manifolds building it. This is due to the fact that the opening is much smaller than in the previous case. Also, there is a significant portion of the repeller in the opening, rendering a morphology which is different from that of the completely open or even the previous case. Again, by taking $a = -0.3$ and eliminating the WGOs, we can see that just two small regions mainly build the repeller, and that they are far from the p_{tr} line [see Fig. 3(d)].

In a recent series of very interesting experiments [17] the emission at the boundary of a partially open BS following Fresnel laws has been studied both theoretically and experimentally. In order to compare with these experimental works, we take $n = 3.3$ (considered in [15]), which is approximately the experimental value and evaluate the same measures as before. In Fig. 4(a) we take $a = 0.3$ to obtain the corresponding LD, which permits one to see the WGOs, as well as more POs

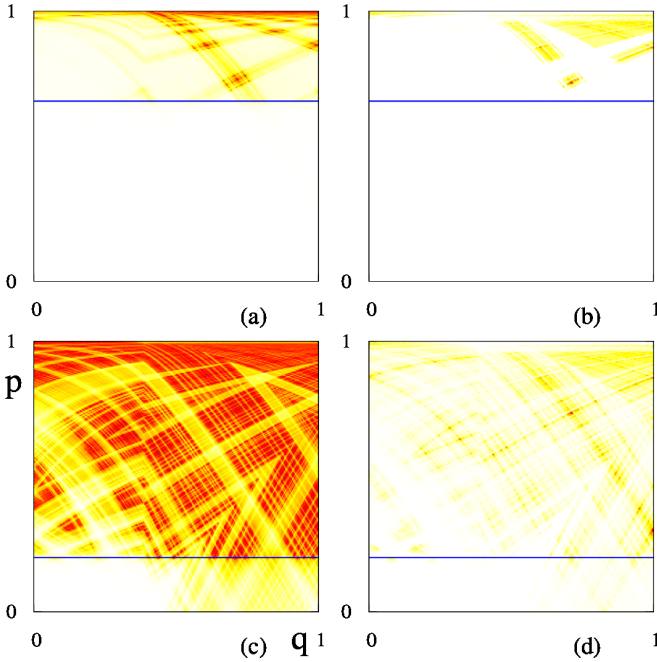


FIG. 3. LD for the partially (Fresnel) open Bunimovich stadium map on the boundary. The left panels correspond to $a = 0.3$ while the right ones to $a = -0.3$. The upper panels show the $n = 1.5$ case and for the lower ones $n = 5.0$. In all panels the value of p_{tr} is indicated by means of blue (black) horizontal lines.

and manifolds building the repeller [less than in the Fig. 3(c) case, though]. As can be seen, there is also a portion of it lying inside the opening. In order to reveal its structure beyond the influence of the WGOs, we again take $a = -0.3$. The corresponding results are shown in Fig. 4(b), where two small regions can be noticed as the major contribution to the repeller structure. One of them is located at both sides of the p_{tr} line (at around $q = 1$). To better understand the physical meaning of this region, we have conducted a systematic search through the first 200 POs of the BS reaching a maximum number of bounces $T = 14$ with the full boundary [see Fig. 1(a)]. We have checked which of them pass through this enhanced region. The results of this search are shown using green (gray) circles in Fig. 4(b). These are all POs that have periodic points in the map on the boundary that are either in the neighborhood of WGOs or around the p_{tr} line.

What do these relevant POs look like? To gain some insight about their morphology, we present them in the left column of Fig. 5, plotted in configuration space, by ascending length order (from top to bottom). The first four are some of the shortest possible POs, and only the last one is a bit longer. Nevertheless, they all share a common main property: they have a large portion that resembles the WGOs, and make one or two bounces near p_{tr} . In fact, they connect the highly confined regions of the repeller with the opening. The desymmetrized version of these POs, shown in the right column, are illustrative of the fact that the economy of computational resources provided by this approach does not affect capturing all features of the dynamics.

Finally, we address an important related point, namely, what is the role played by these POs (and its neighboring

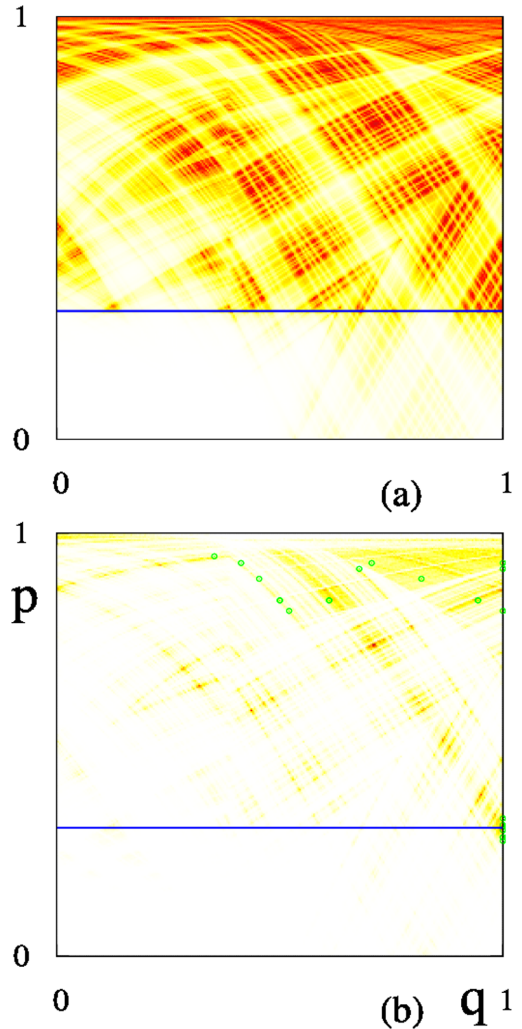


FIG. 4. LD for the partially open Bunimovich stadium map on the boundary, following Fresnel's laws with $n = 3.3$. The value of p_{tr} is indicated by means of blue (black) horizontal lines. In (a) $a = 0.3$ and in (b) $a = -0.3$. The green (gray) circles in (b) show all the periodic points associated to the shortest POs that pass through the enhanced region around p_{tr} .

region/homoclinic tangle) in the microlaser emission. To answer this question, we have calculated the unstable manifold of the partially open BS using the LD^+ measure; the results are shown in Fig. 6(a). Besides the fact that most of the escape from the repeller happens at the circular part of the boundary, it is hard to see any finer structure associated to a given value of q . Moreover, it is worth noticing that determining the structure of this manifold is not always straightforward [17,20]; however, the LDs used here allowed us to do that in an extremely simple way. Also recall that the unstable manifold method [21–23] is widely accepted in order to make a theoretical prediction of the microlasers emission patterns [20], at least when the wavelength is much smaller than the cavity size, i.e., deep in the semiclassical regime. In this respect, some works focused on the inner structure of the emission, pointing toward POs of interest. In [24] the directionality of the far-field emission was related to very short POs, in particular the rectangle orbit of a specific case of the BS

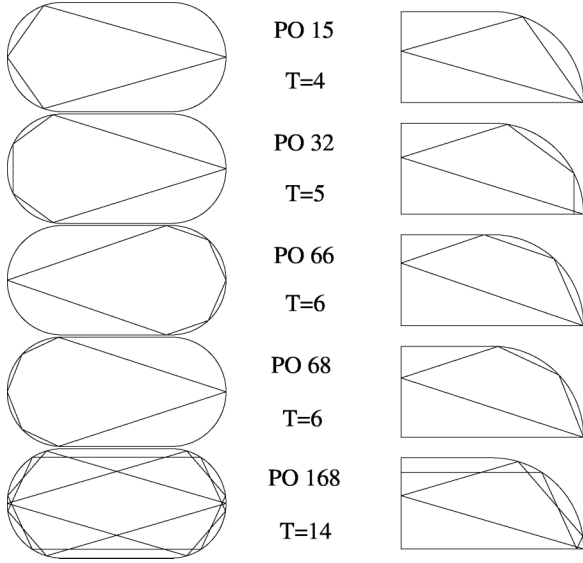


FIG. 5. Shortest POs that pass through the enhanced region of LD around p_{tr} shown in Fig. 4(b). In the left and right columns the full and desymmetrized Bunimovich stadium versions, respectively, are shown. The POs are ordered according to their lengths, and the number of bounces T for the full case is indicated for each one of them. Notice that PO 168 is the only fully symmetrical (with respect to horizontal and vertical reflections) PO; we show an example of a symmetry-related partner by means of PO 66.

with a short straight segment (thought of as a deformation of boundaries associated to mixed phase spaces). Also, in [25] a stable rectangle PO plays a central role in a mixed dynamical scenario (and in the quantum regime). We next make systematic our analysis by calculating the short time forward evolution of 10^6 random initial conditions, located in small domains around p_{tr} in phase space. We call this Liouville distribution $L(q, p)$ (notice that for Lagrangian descriptors we use the notation LD instead). We consider rectangles of a size given by one region X_i along q and nine along p , centered at p_{tr} and at $q_{ic} = 0.1, \dots, 1.0$ with $\Delta q = 0.1$. The evolution is then carried out up to $t_f = 14$, which is the maximum number of trajectory bounces allowed in our previous search. The results are shown in Figs. 6(b) and 6(c), where we can see two significant examples of this. In the first case $q_{ic} = 0.2$ was considered for the initial distribution, while in the second case $q_{ic} = 1.0$ (see the small rectangles around p_{tr}). It is clear that for the smaller q_{ic} value the evolved density does not reveal the features of the emission region of the repeller, while it does for $q_{ic} = 1.0$. Obviously, some differences are observed between the two cases, and we do not claim that just a single orbit is responsible for all of the emission, but we do think that a small set of them associated to a homoclinic tangle can provide a very complete approximation to its structure. As a matter of fact, if we look at results in Fig. 6(d), it can be seen that the normalized cumulative distribution in the opening $D = \int_{-p_{tr}}^{p_{tr}} L dp$ as a function of q resembles that of the complete unstable manifold $D = \int_{-p_{tr}}^{p_{tr}} LD^+ dp$. We also plot the same results for the completely open scenario where the behavior is generally similar but with some differences due to the fact that a discontinuous function has been taken for the

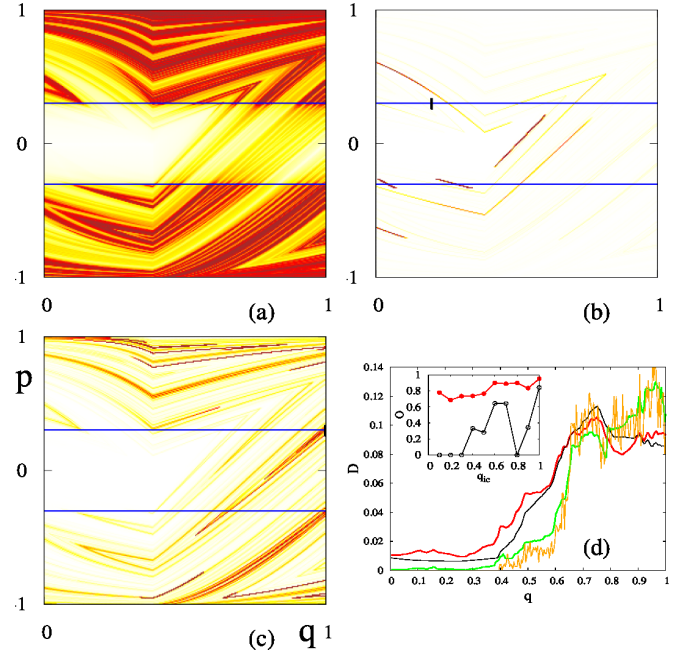


FIG. 6. (a) LD^+ for the partially open Bunimovich stadium map on the boundary, following Fresnel's laws with $n = 3.3$, which corresponds to the unstable manifold. In (b) and (c), L distributions of 10^6 random initial conditions located at the black rectangles around p_{tr} ($q_{ic} = 0.2$ and $q_{ic} = 1.0$, respectively) and evolved up to time $t_f = 14$ are shown. In all cases, the values of $\pm p_{tr}$ are indicated by means of blue (black) horizontal lines. (d) Normalized distribution D at the opening region (from $-p_{tr}$ to p_{tr}) as a function of q for the LD^+ in (a) [red (dark) line for the Fresnel opening and thin black line for the corresponding distribution in the complete opening case] and for the distribution in (c) [green (gray) line for the Fresnel opening and thin orange (light gray) line for the complete opening]. In the inset we show the overlap O (restricted to the opening) between the LD^+ and similar distributions to those in (b) and (c) but for different values of q_{ic} [red (dark) line with filled circles for the Fresnel opening and thin black line with empty circles for the corresponding distributions in the complete opening case].

opening. This introduces more fluctuations, especially for the case of the small rectangles evolution. In the inset we see that the overlap $O = \int_{-p_{tr}}^{p_{tr}} \int_q LD^+ \times L dq dp$ between the full distributions in the escaping region corresponding to the unstable manifold and those at different q_{ic} are the worst for $q_{ic} = 0.2$ and the best for $q_{ic} = 1.0$, reaching here a remarkable 0.95 value in the Fresnel opening case. A similar behavior is found in the completely open setting, but the worst results are now enhanced by the lack of smoothing of the fractal structure of the manifold, i.e., when the initial conditions are located at an empty region they just disappear through the hole, and nothing is reflected.

IV. CONCLUSIONS

In this work we have extended the application of the LD classical measure to realistic open systems. By considering the partially open BS with Fresnel's laws we have addressed an issue of great experimental interest, such as the emission properties of microlasers and dielectric resonant cavities in

general [17,25]. Nevertheless the LDs of the closed system proved very useful in understanding the central role played by BBOs, followed in relevance by the WGOs and their associated manifolds, in structuring the chaotic phase space. Opening the system induces the formation of a repeller whose main characteristic is the lack of the BBOs and their main manifolds, whose role is now taken over by the WGOs.

By using our definition of LDs for open systems [13] we were able to unveil the inner structure of the repeller, especially in the escaping region. We have been able to identify a set of short POs that pass through a small enhanced region of the repeller that is located near $q = 1.0$ and $p = p_{tr}$. We have found that they share the same morphology, being a kind of hybrid between WGOs (that act as a sort of reservoir) and escaping trajectories. Given that the partially open BS microlaser emission on the boundary [17] can be determined by means of the unstable manifold calculation, we have computed this magnitude by using our measure in a very straightforward way. Moreover, we compared this distribution with the ones obtained by means of a short time evolution of initial conditions very close to the POs identified thanks to the LDs. We have been able to quantitatively demonstrate in this way that these POs provide all the relevant structure of

the escaping portion of the repeller. This leads us to conclude that the interplay between the shape of the microcavity and the index of refraction n can single out a small group of short POs than can very well approximate the emission properties in chaotic systems. Our method provides a systematic way to find them. This is a very important result that should have a large influence in the future design of microlasers [26,27].

Finally, we think that this work could be of relevance at the time of considering smaller cavities, where a purely classical calculation would not be enough to describe them. In that scenario, the semiclassical theory of short POs [18,19] will benefit from the identification of those orbits outside of the completely open repeller that significantly contribute to construct the partially open one in realistic situations.

ACKNOWLEDGMENTS

Support from CONICET is gratefully acknowledged. This research has also been partially funded by the Spanish Ministry of Science, Innovation and Universities, Gobierno de España under Contract No. PGC2018-093854-B-I00, and by ICMAT Severo Ochoa Programme for Centres of Excellence in R & D (CEX2019-000904-S).

-
- [1] J. A. Jiménez-Madrid and A. M. Mancho, *Chaos* **19**, 013111 (2009).
- [2] A. M. Mancho, S. Wiggins, J. Curbelo, and C. Mendoza, *Commun. Nonlinear Sci. Numer. Simul.* **18**, 3530 (2013).
- [3] F. Balibrea-Iniesta, C. Lopesino, S. Wiggins, and A. M. Mancho, *Int. J. Bifur. Chaos* **25**, 1550172 (2015).
- [4] J. Montes, F. Revuelta, and F. Borondo, *Commun. Nonlinear Sci. Numer. Simul.* **102**, 105860 (2021).
- [5] L. Wenyang, N. Shibabrat, and S. Wiggins, *Commun. Nonlinear Sci. Numer. Simul.* **103**, 105949 (2021).
- [6] F. Revuelta, R. M. Benito, and F. Borondo, *Phys. Rev. E* **99**, 032221 (2019).
- [7] A. Junginger, G. T. Craven, T. Bartsch, F. Revuelta, F. Borondo, R. M. Benito, and R. Hernandez, *Phys. Chem. Chem. Phys.* **18**, 30270 (2016).
- [8] S. Patra and S. Keshavamurthy, *Phys. Chem. Chem. Phys.* **20**, 4970 (2018).
- [9] F. Revuelta, R. M. Benito, and F. Borondo, *Phys. Rev. E* **104**, 044210 (2021).
- [10] V. J. García-Garrido, F. Balibrea-Iniesta, S. Wiggins, A. M. Mancho, and C. Lopesino, *Regul. Chaotic Dyn.* **23**, 751 (2018).
- [11] K. Clauß, E. G. Altmann, A. Bäcker, and R. Ketzmerick, *Phys. Rev. E* **100**, 052205 (2019).
- [12] B. R. Hunt, E. Ott, and J. A. Yorke, *Phys. Rev. E* **54**, 4819 (1996); Y.-C. Lai and T. Tél, *Transient Chaos, Complex Dynamics on Finite-Time Scales* (Springer, New York, 2011).
- [13] G. G. Carlo and F. Borondo, *Phys. Rev. E* **101**, 022208 (2020).
- [14] M. Novaes, *J. Phys. A: Math. Theor.* **46**, 143001 (2013).
- [15] J. Wiersig and J. Main, *Phys. Rev. E* **77**, 036205 (2008).
- [16] J. Kullig and J. Wiersig, *New J. Phys.* **18**, 015005 (2016).
- [17] S. Bittner, K. Kim, Y. Zeng, Q. J. Wang, and H. Cao, *New J. Phys.* **22**, 083002 (2020).
- [18] G. G. Carlo, R. M. Benito, and F. Borondo, *Phys. Rev. E* **94**, 012222 (2016).
- [19] C. A. Prado, G. G. Carlo, R. M. Benito, and F. Borondo, *Phys. Rev. E* **97**, 042211 (2018).
- [20] E. G. Altmann, J. S. E. Portela, and T. Tél, *Rev. Mod. Phys.* **85**, 869 (2013).
- [21] J. U. Nöckel, A. D. Stone, and R. K. Chang, *Opt. Lett.* **19**, 1693 (1994).
- [22] J. U. Nöckel, A. D. Stone, G. Chen, H. L. Grossman, and R. K. Chang, *Opt. Lett.* **21**, 1609 (1996).
- [23] J. U. Nöckel and A. D. Stone, *Nature (London)* **385**, 45 (1997).
- [24] H. G. L. Schwefel, N. B. Rex, H. E. Tureci, R. K. Chang, A. D. Stone, T. Ben-Messaoud, and J. Zyss, *J. Opt. Soc. Am. B* **21**, 923 (2004).
- [25] S. Shinohara, T. Harayama, T. Fukushima, M. Hentschel, T. Sasaki, and E. E. Narimanov, *Phys. Rev. Lett.* **104**, 163902 (2010).
- [26] A. Li, K. Tian, J. Yu, R. A. Minz, J. M. Ward, S. Mondal, P. Wang, and S. N. Chormaic, *Opt. Exp.* **29**, 16879 (2021).
- [27] L. Andreoli, X. Porte, T. Heuser, J. Große, B. Moeglen-Paget, L. Furfaro, S. Reitzenstein, and D. Brunner, *Opt. Express* **29**, 9084 (2021).